

Phase Transitions in Hexane Monolayers Physisorbed onto Graphite

M.W. Roth and C.L. Pint

Department of Physics, University of Northern Iowa, Cedar Falls, Iowa 50614

Carlos Wexler

Department of Physics and Astronomy, University of Missouri-Columbia, Columbia, Missouri 65211

(Dated: February 8, 2020)

We report the results of molecular dynamics (MD) simulations of a complete monolayer of hexane physisorbed onto the basal plane of graphite. At low temperatures the system forms a herringbone solid. With increasing temperature, a solid to nematic liquid crystal transition takes place at $T_1 = 138 \pm 2\text{K}$ followed by another transition at $T_2 = 176 \pm 3\text{K}$ into an isotropic fluid. We characterize the different phases by calculating various order parameters, coordinate distributions, energetics, spreading pressure and correlation functions, most of which are in reasonable agreement with available experimental evidence. In addition, we perform simulations where the Lennard-Jones interaction strength, corrugation potential strength and dihedral rigidity are varied in order to better characterize the nature of the two transitions through. We find that both phase transitions are facilitated by a “footprint reduction” of the molecules via tilting, and to a lesser degree via creation of gauche defects in the molecules.

PACS numbers: 64.70.-p, 68.35.Rh, 68.43.-h

I. INTRODUCTION

The physical adsorption (physisorption) of atoms and molecules onto a substrate to form a quasi two-dimensional (2D) film has resulted in the observation of a rich variety of behavior not realized in the system’s corresponding three-dimensional (3D) or “bulk” state.

Among the species used as adsorbates, alkanes are of considerable interest because of their technological importance (e.g. as lubricants) and because they are among the simplest families of molecules of compounds whose members differ mainly in their length. In fact, straight-chained n-alkanes represent a fine balance between complexity (i.e. many internal degrees of freedom which also affect the interaction *between* molecules) and the simplicity of their structure (as compared to other organic molecules). In fact, over the past decades there has been a constant and renewed effort to better understand the adsorption of alkanes over a variety of substrates. Among the substrates used for physisorption studies, graphite, with its excellent mechanical stability, availability and symmetry, has proven to be one of the best choices. A considerable amount of experimental, theoret-

ical and computational work has, thus, been devoted to these studies.

Hexane on graphite was first studied by Krim *et al.*¹ using LEED as well as neutron diffraction. For submonolayer coverage a uniaxial incommensurate (UI) herringbone phase is observed below ca. $T = 151\text{ K}$, where a first-order melting transition is found (but note that but a determination of the molecular orientations was not possible). At low temperatures, as the coverage is increased, the UI phase evolves continuously into a $2 \times 4\sqrt{3}$ commensurate structure at completion. More recently, Taub and co-workers² completed extensive neutron^{2,3} and X-ray² diffraction studies of hexane on graphite for submonolayer², monolayer²⁻⁶ and multilayer² coverages. Their findings indicate that at low temperatures a complete monolayer forms a commensurate herringbone structure which evolves with increasing temperature into a rectangular centered solid/liquid coexistence region by ca. 150 K and melts at around 175 K²⁻⁶. For submonolayer coverages, these authors proposed a structure corresponding to a UI phase comprised of commensurate regions separated by low-density fluid filled domain walls².

In the 1990's, Hansen *et al.* reported studies combining MD computer simulations with neutron and x-ray diffraction studies of butane and hexane on graphite at monolayer completion^{4,5}. Experimentally, butane melts abruptly at around $T = 116$ K directly from a solid commensurate rectangular-centered herringbone (HB) phase into a liquid. Orientational ordering about the surface normal is lost through rotation about the center of mass, which is simultaneous with melting. Hexane, on the other hand, undergoes a loss of translational order at about 150 K into a phase with short-range order which is thought to involve mobile rectangular-centered (RC) islands within a fluid. Then, at around $T = 175$ K the system melts into a fluid.

The computer simulations of Hansen *et al.*^{4,5} showed that, for hexane, the internal formation of *gauche* defects coupled with out-of-plane tilting is concurrent with melting. The necessary creation of in-plane room by either *gauche* defects or tilting at the onset of melting is referred to as a “footprint reduction” mechanism. These simulations showed, furthermore, that the nature and temperature of the transition is very sensitive to the presence of *gauche* defects, as the melting temperature raises drastically when *gauche* defect formation is suppressed. However, the resulting melting temperature of a hexane monolayer was found to be 222 K, significantly different from the experimental value of 175 K. This discrepancy was addressed in a series of MD simulations of hexane on graphite by Velasco and Peters⁷ which found a better agreement with experimental values of the melting temperature when a considerably lower adsorbate-interaction strength was used, and under those conditions molecular *gauche* defect formation becomes almost irrelevant to melting. (In this paper we find the presence of an intermediate nematic phase. In the herringbone solid to nematic phase transition we find *gauche* defects to be irrelevant. For the nematic to isotropic liquid phase transition, we find that both mechanisms contribute to the “footprint reduction”, although it is apparent that tilting is the dominant effect.)

More recently, Peters and coworkers have also examined the behavior of monolayer⁸ and bilayer⁹ hexane on graphite using MD simulation

techniques. The monolayer study compared MD results based on the standard (isotropic) unified atom (UA) approximation to simulations where an *anisotropic* force field was employed. Using a computational cell of 112 hexane molecules, and performing MD simulations corresponding to 200,000 steps of 1 fs both models yielded the same basic physics, especially in regards to the characterization of the phases observed (the transition temperature from commensurate herringbone to the rectangular centered orientationally ordered phase is found at around 150 K and the melting temperature at 175 K in both cases, the main difference between the two models is that the anisotropic model promotes more in-plane mobility from vacancy creation due to increased molecule tilting at all temperatures).

Even though hexane on graphite has been studied quite well experimentally, it has not been as thoroughly investigated computationally, and there is still some doubt about the roles played in the phase transitions by the internal degrees of freedom of the molecules (mainly *gauche* defects) and their relative importance as the adatom-substrate interaction is varied. Furthermore, it is not self-evident that the simulations have achieved ergodicity to a satisfactory degree, as only a relatively limited simulation time has been explored so far (maximum of 2 ns in reference 8). The general purpose of the work reported here is to enrich our understanding of phase transitions in physisorbed molecular systems, in particular of hexane in graphite. Specifically, we wish to: (i) more sharply delineate the phase transitions of hexane on graphite using longer simulations (up to 5 times longer than previously reported); (ii) to understand the effects of varying the graphite corrugation strength and the adatom-adatom interaction strength on the observed phase transitions; (iii) to further delineate the role of the internal degrees of freedom of the adsorbed molecules, i.e. the bond bending and dihedral torsion in the observed phase transitions, and (iv) to gain insight in the energetics and possible mechanisms for the observed phase transitions.

Since the system under consideration is, to some degree, (quasi-) two-dimensional, one may have expected that the observed phase transi-

tions would show some of the universal features expected from the beautiful theory of 2D melting developed in the 1970's by Kosterlitz, Thouless, Halperin, Nelson and Young^{10–14}. However, the importance of the out-of-plane behavior of the hexane monolayer, and the “polarizing” effect of the substrate corrugation make it difficult to reliably place these transitions in a general theoretical context. Furthermore, it is evident that the relatively small system sizes achievable in MD simulations does not permit a complete characterization of the phase transitions observed (e.g. their order), but sometimes the modality of energy distributions near the critical regions may give *indications* on what behavior to expect.

The paper is organized as follows. In Sec. II we discuss the computer simulation procedures. The results of the simulations are presented in Sec. III, and are discussed in detail in Sec. IV.

II. COMPUTATIONAL DETAILS

The hexane molecules in our study are modeled with two methyl (CH₃) pseudo atoms on its ends and four methylene (CH₂) pseudo atoms in between. The lowest energy conformation of the molecule consists of all pseudo atoms being co-planar, forming a zig-zag pattern with 114° three-body bond angles (dihedral angles) and bond lengths (nearest neighbor separations) of 1.54 Å. In the simulations that follow we keep the the bond lengths fixed, but allow the other internal degrees of freedom to vary (bond angle bending and dihedral angle torsion). The graphite substrate modeled as being static, containing an infinite number of stacked graphene sheets (see Fig. 1). The structure contains point carbon atoms at the vertices of all bonds and the bond length is taken to be 2.46 Å.

A. Method

A constant particle number, planar density and temperature ($N = 672$, $\rho = 1$, T) molecular dynamics (MD) method is employed to conduct atomistic simulations a system of $N_m = 2 \times m \times n = 112$ hexane molecules at monolayer completion ($m = 4$ and $n = 14$). The rectan-

gular computational cell (see Figure 1) has its corners coincident with graphite hexagon centers and has dimensions $m \times 4\sqrt{3}a \simeq 68.1735$ Å and $n \times 2a = 68.88$ Å in the x and y directions respectively. Such a cell gives a planar density of $\rho = 0.02385$ molecules/Å² and an area per molecule of 42 Å². Each hexane molecule consists of six united atom (UA) pseudoatoms—two methyl (CH₃) and four methylene (CH₂). Periodic boundary conditions are utilized for each pseudoatom in the x, y directions and free boundary conditions are present in the vertical z direction. To perform the simulations at constant temperature, we periodically rescale the velocities so that equipartition is satisfied for the center-of-mass, rotational and internal temperatures:

$$\begin{aligned} T_{CM} &= \frac{1}{3N_mk_B} \sum_{i=1}^{N_m} M_i v_{i,CM}^2, \\ T_{ROT} &= \frac{1}{3N_mk_B} \sum_{i=1}^{N_m} \boldsymbol{\omega}_i^T \mathcal{I}_i \boldsymbol{\omega}_i, \\ T_{INT} &= \frac{1}{(2n_C - 5)N_mk_B} \sum_{i=1}^{N_m} \sum_{j=1}^{n_C} m_{ij} \\ &\quad \times [(\mathbf{v}_{ij} - \mathbf{v}_{i,CM}) - \boldsymbol{\omega}_i \times (\mathbf{r}_{ij} - \mathbf{r}_{i,CM})]^2, \end{aligned} \quad (1)$$

respectively (no significant differences were found when “thermalizing” a subset of the temperatures above). Here N_m is the number of molecules, n_C the number of pseudoatoms per molecule, the i index runs over the molecules ($1 \leq i \leq N_m$) and the j index runs over the pseudoatoms within a given molecule ($1 \leq j \leq n_C$). Furthermore, for each molecule, M_i is the mass, $\mathbf{v}_{i,CM}$ is the center-of-mass velocity, $\boldsymbol{\omega}_i$ is the angular velocity and \mathcal{I}_i is the moment of inertia tensor (relative to the COM). Last, \mathbf{v}_{ij} is the velocity of the j -th pseudoatom in the i -th molecule, and k_B is Boltzmann’s constant.

The time step for all simulations is chosen to be 1 fs and integration of the equations of motions is achieved with a velocity Verlet RATTLE¹⁵ algorithm which keeps the pseudoatom bond lengths constant. Runs are typically started from a herringbone configuration, as suggested by experimental evidence (e.g. the neutron diffraction data of Ref. 1), and allowed to equilibrate for roughly $3\text{--}5 \times 10^5$ steps, aver-

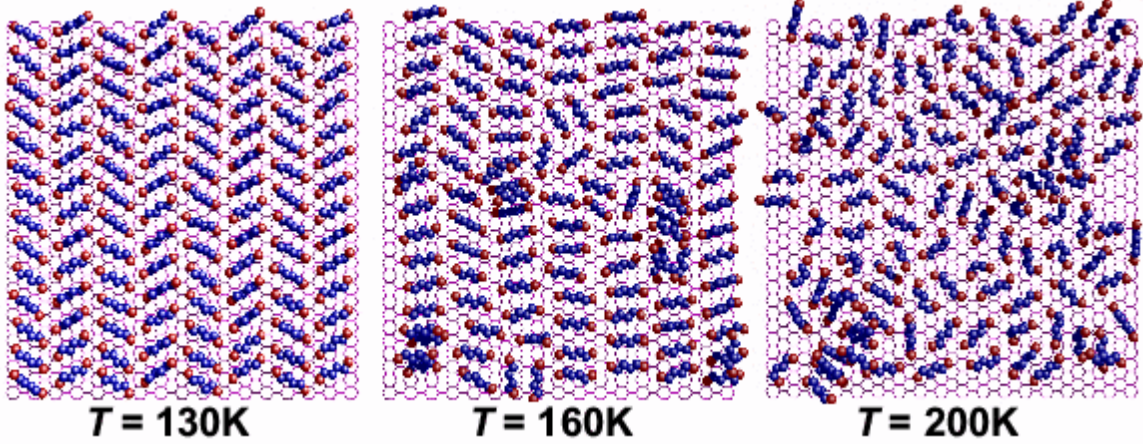


FIG. 1: Simulation cell showing snapshots of typical (equilibrium) configurations for the hexane/graphite system in the commensurate herringbone solid ($T = 130$ K), the orientationally ordered nematic ($T = 160$ K) and isotropic liquid ($T = 200$ K) phases. CH_3 end-of-chain pseudoatoms are red, CH_2 are yellow and the C-C bonds in the graphite substrate are purple (the graphite lattice spacing is $a = 2.46$ Å). The computational cell has dimensions $m \times 4\sqrt{3}a \simeq 68.1735$ Å and $n \times 2a = 68.88$ Å in the x and y directions respectively, where $m = 4$ and $n = 14$, and periodic boundary conditions are used in x and y directions. There are $2 \times m \times n = 112$ hexane molecules.

ages are taken for $0.5\text{--}1.0 \times 10^6$ steps after equilibration. Some runs are started from the final configuration of some lower temperature run. A good measure of convergence is that incorporating the results from both types of initial conditions does not create noticeable scatter in the results. The only hysteresis observed is that, as is usual in these type of simulations, “freezing” by starting from a high temperature phase and lowering the temperature is not readily achieved.

B. Interaction Potentials

The model adopted for our study of adsorbed hexane molecules on graphite corresponds to having both non-bonded and bonded interactions. The first of two non-bonded interactions is the adsorbate-adsorbate interaction between pseudoatom atom i and j separated by a distance r_{ij} , which is modeled by a Lennard-Jones pair potential

$$u_{LJ}(r_{ij}) = 4\epsilon_{ij} \left[\left(\frac{\sigma_{ij}}{r_{ij}} \right)^{12} - \left(\frac{\sigma_{ij}}{r_{ij}} \right)^6 \right]. \quad (2)$$

Lorentz-Bertholot combining rules

$$\sigma_{ij} = \frac{\sigma_i + \sigma_j}{2}, \quad \epsilon_{ij} = \sqrt{\epsilon_i \epsilon_j}, \quad (3) \quad \text{with}$$

are applied in order to describe mixed interactions when particles i and j are of different types; lattice sums are taken out to 10 Å and values for the potential parameters used in our work¹⁶ are given in Table I.

The second non-bonded interaction is the adatom-graphite interaction. The graphite is modeled as being of infinite extent in the xy plane and semi-infinite in the vertical $-z$ direction. The adatom-graphite interaction potential, however, is not taken as a discrete sum over the carbon atoms. Steele’s expansion¹⁷ is utilized because it exploits the fact that the symmetry of the substrate breaks the adatom-graphite interaction into a vertically (laterally averaged) portion and a much weaker portion related to the undulation in the interaction due to the graphite hexagonal symmetry. Such a representation saves a considerable amount of computing time. In other words, the interaction of the adsorbate atoms with the substrate is the Fourier expansion

$$u_{gr}(\mathbf{r}_i) = E_{0i}(z_i) + \sum_{n=1}^{\infty} E_{ni}(z_i) f_n(x_i, y_i), \quad (4)$$

$$\begin{aligned}
E_{0i}(z_i) &= \frac{2\pi q \epsilon_{gr} \sigma_{gr}^6}{a_s} \left[\frac{2\sigma_{gr}^6}{45d(z_i + 0.72d)^9} + \frac{2\sigma_{gr}^6}{5z_i^{10}} - \frac{1}{z_i^4} - \frac{2z_i^2 + 7z_id + 7d^2}{6d(z_i + d)^5} \right], \\
E_{ni}(z_i) &= \frac{2\pi \epsilon_{gr} \sigma_{gr}^6}{a_s} \left[\left(\frac{\sigma_{gr}^6}{30} \right) \left(\frac{g_n}{2z_i} \right)^5 K_5(g_n z_i) - 2 \left(\frac{g_n}{2z_i} \right)^2 K_2(g_n z_i) \right], \\
f_1(x_i, y_i) &= 2 \cos \left[\frac{2\pi}{a} \left(x + \frac{y}{\sqrt{3}} \right) \right] + 2 \cos \left[\frac{2\pi}{a} \left(x - \frac{y}{\sqrt{3}} \right) \right] + 2 \cos \left[\frac{4\pi}{a} \left(\frac{y}{\sqrt{3}} \right) \right],
\end{aligned} \tag{5}$$

TABLE I: Non-bonded potential parameters used in the simulations

Parameter	Value
$\epsilon_{\text{CH}_2}, \epsilon_{\text{CH}_3}$	72 K
$\sigma_{\text{CH}_2}, \sigma_{\text{CH}_3}$	3.92 Å
q	2
a	2.46 Å
a_s	5.24 Å ²
d	3.357 Å
ϵ_{gr}	44.89 K
σ_{gr}	3.66 Å

Here g_n is the modulus of the n -th graphite reciprocal lattice vector and the $K_n(x)$ are modified Bessel functions of the second kind. The interaction is obtained by summing over an infinite number of graphene sheets. Only $f_1(x_i, y_i)$ is defined above because the sum in x, y -dependent part of equation (4) converges extremely rapidly and only the $n = 1$ term is needed. All potential parameters for the adsorbate-substrate interaction are identified in Table I.

There are two types of bonded interactions considered in this work: bond angle bending and dihedral angle bending (we assume that the bond lengths are fixed at 1.54 Å, the RATTLE algorithm allows for constrained solution of the equation of motion¹⁵). The bond angles are assumed to be harmonic; their bending potential energy comes from Martin and Siepmann¹⁶ and is given by

$$u_{bend}(\theta_b) = \frac{k_\theta}{2} (\theta_b - \theta_0)^2, \tag{6}$$

where θ_b is the bond angle, θ_0 is the equilibrium

bond angle and k_θ is the angular stiffness. In addition, the expression for the energy of dihedral bending (torsion)^{8,18} is of the form

$$u_{tors}(\phi_d) = \sum_{i=0}^5 c_i (\cos \phi_d)^i, \tag{7}$$

where ϕ_d is the dihedral angle and the c_i are constants. All values for the bonded potential parameters are shown in Table II. This potential has one global minimum for the *trans* configuration $\phi_d = 0$ and two local minima with ~ 234 K higher in energy for the two *gauche* configurations at $\phi_d = \pm 2\pi/3$.

The full potential energy can thus be written:

$$U = U_{nb} + U_b, \tag{8}$$

$$\begin{aligned}
U_{nb} &= \frac{1}{2} \sum'_{i,i'=1}^{N_m} \sum_{j,j'=1}^{n_C} u_{LJ}(|\mathbf{r}_{ij} - \mathbf{r}_{i'j'}|) + \sum_{k=1}^N u_{gr}(\mathbf{r}_k), \\
U_b &= \sum_{i=1}^{N_m} \left[\sum_{j=1}^{n_C-2} u_{bend} + \sum_{j=1}^{n_C-3} u_{tors} + \sum_{j=1}^{n_C-4} u_{LJ} \right].
\end{aligned}$$

TABLE II: Bonded potential parameters used in the simulations

Parameter	Value
k_θ	62,793.6 K/rad ²
θ_0	114°
c_0	1,037.76 K
c_1	2,426.07 K
c_2	81.64 K
c_3	-3,129.46 K
c_4	-163.28 K
c_5	-252.73 K

III. RESULTS

We performed MD simulations as described above for many temperatures in the 100–200 K range. Figure 1 shows snapshot of typical configurations of the simulated hexane/graphite system for three characteristic temperatures where the herringbone (HB) commensurate solid, the “nematic,” and the fluid phases are observed. It should be mentioned that promotion of molecules to higher layers was not very significant at any of the temperatures studied. From this figure it is evident that in the low-temperature phase molecules are arranged in a HB structure where the molecules’ azimuthal angles $\phi_i \in [0, \pi]$ ¹⁹ take predominantly values near $\{30^\circ, 150^\circ\}$ (ϕ_i is defined as the angle that the axis of the smallest moment of inertia for molecule i makes with the x -axis). Moreover, the molecules are in registry with the substrate. Clearly this HB phase is solid. In the high-temperature regime, it is also quite clear that the molecules are randomly positioned and oriented (and in particular not in registry with the substrate), which is strongly suggestive of a liquid phase. The situation of the mesophase, however, is not as evident. It is clear that it has a definite orientational order, quite different than the HB (most azimuthal angles centered around 0° , the molecules appear not to be commensurate with the substrate, and it is not clear whether the system is in a liquid crystalline state (i.e. a *nematic*), or in a solid phase (i.e. a rectangular centered solid). The exact nature of the different phases (and in particular of the mesophase) is addressed more quantitatively below, by means of examination of various order parameters, energy analysis, spreading pressure, distributions and correlation functions.

A. Order parameters

Figure 2 shows the temperature dependence of several molecular order parameters which are useful in characterizing the system’s behavior through and across phases. The herringbone order parameter is used to quantify the in-plane orientational ordering of the molecular axes and is defined as

$$OP_{herr} \equiv \frac{1}{N_m} \left\langle \sum_{i=1}^{N_m} (-1)^j \sin(2\phi_i) \right\rangle, \quad (9)$$

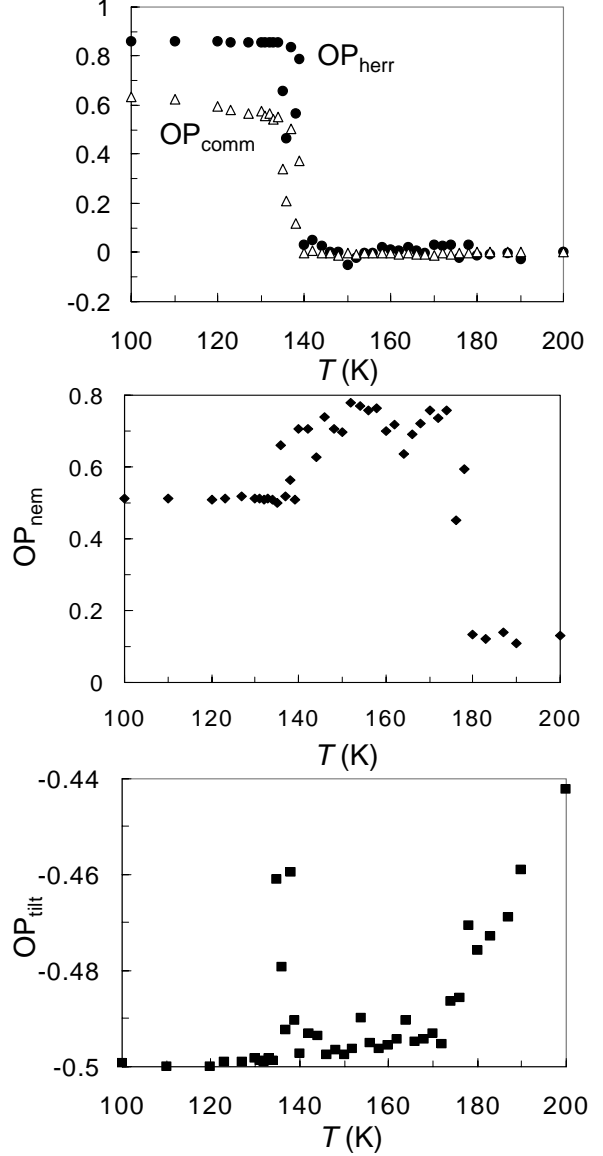


FIG. 2: Structural order information. The following order parameters (OP) are presented as functions of temperature: Herringbone OP_{herr} (solid circles), center of mass OP_{comm} (open triangles), nematic OP_{nem} (solid diamonds) and tilt OP_{tilt} (solid squares) .

where the sum is performed over all molecules, the integer j is assigned so as to take the two sublattices into account and the averages correspond to sampling a large number of uncorrelated configurations in each MD simulation. For a “perfect herringbone” with $\phi_i \in \{45^\circ, 135^\circ\}$, $OP_{herr} = 1$, obviously OP_{herr} vanishes if the two sublattices cannot be distinguished (e.g. if all angles are clustered around *one* angle or if all an-

gles are sampled equally) either statically (over the lattice) or dynamically (over time). For the HB phase, where the ϕ_i 's are clustered around 30° and 150° (for further evidence see the 130 K curve in Fig. 7), we find $OP_{herr} \simeq \sqrt{3}/2 \simeq 0.866$, as observed for temperatures smaller than $T_1 = 138 \pm 2$ K. Not surprisingly $OP_{herr} \simeq 0$ for the high temperature phase as essentially all azimuthal angles are equally sampled (see the 200 K curve in Fig. 7). We also find $OP_{herr} \simeq 0$ for the mesophase, which is also evident from the ϕ_i distributions which show a single significant orientation and thus the lack of two angular distinct sublattices (see the 160 K curve in Fig. 7).

To investigate whether the adsorbed molecules are in registry with the graphite substrate we also measure the commensurate order parameter OP_{comm} , defined as

$$OP_{comm} \equiv \frac{1}{6N_m} \left\langle \sum_{i=1}^{N_m} \sum_{s=1}^6 e^{-i\mathbf{g}_s \cdot \mathbf{r}_i} \right\rangle, \quad (10)$$

where the outer sum runs over all N_m molecules at center-of-mass position \mathbf{r}_i , and the inner sum runs over all six graphite reciprocal lattice vectors $\mathbf{g}_s \in \{(\pm\pi/3a, 0), (\mp\pi/6a, \pm\pi/\sqrt{3}a), (\pm\pi/6a, \pm\pi/\sqrt{3}a)\}$. OP_{comm} takes on a value of unity were all molecular centers to remain statically graphite hexagon centers and vanishes in the limiting case of the molecular centers uniformly sampling positions in the xy plane. As with OP_{herr} , Such a sampling could occur either in a static fashion (an infinite incommensurate solid) or in a dynamic fashion such as in a non-registered film. It is evident from Fig. 2, that as the HB phase disappears at $T_1 = 138 \pm 2$ K, the film also loses registration with the substrate. This is also evident in the decrease of the corrugation energy (see Sec. IIIB and bottom panel of Fig. 3).

Both OP_{herr} and OP_{comm} are useful in providing information on the solid to nematic transition at $T_1 = 138 \pm 2$ K but are unable to provide any characterization of the nematic to isotropic liquid transition. The nematic order parameter OP_{nem} provides precisely the needed information and is defined by

$$OP_{nem} \equiv \frac{1}{N_m} \left\langle \sum_{i=1}^{N_m} \cos 2(\phi_i - \phi_{dir}) \right\rangle, \quad (11)$$

where ϕ_{dir} is an “average” azimuthal direction defined by maximizing the nematic order parameter: $\partial OP_{nem} / \partial \phi_{dir} \equiv 0$:

$$\phi_{dir} = \frac{1}{2} \tan^{-1} \left[\frac{\sum_{i=1}^{N_m} \sin 2\phi_i}{\sum_{i=1}^{N_m} \cos 2\phi_i} \right]. \quad (12)$$

Note that due to the $1/2$ pre-factor, it is important to use the 4-quadrant version of the \tan^{-1} function to uniquely define ϕ_{dir} (the 2-quadrant version leads to the possibility of $\pi/2$ rotations which are relevant for the final value of OP_{nem} in some cases).

The center panel of Fig. 2 shows the temperature dependence of the nematic order parameter. This order parameter clearly indicates that, in addition to the HB to nematic phase transition at $T_1 = 138 \pm 2$ K, a second *orientational* phase transition occurs at $T_2 = 176 \pm 3$ K. As shown earlier for the OP_{herr} , OP_{nem} also is clearly correlated to the azimuthal angle distributions (Fig. 7). For a “perfect herringbone” solid ($OP_{herr} = 1$), ϕ_{dir} is completely *undefined* and OP_{nem} vanishes, but for the solid commensurate herringbone phase of hexane on graphite ($OP_{herr} = \sqrt{3}/2$), $\phi_{dir} = 0$ and the limiting value of OP_{nem} is 0.5. In a perfect nematic phase, all molecules share the same orientation and $OP_{nem} = 1$. Our results of $\max[OP_{nem}] \simeq 0.8$ show the presence of significant fluctuations in the molecular orientations and of the presence of differently oriented domains, both features are also clearly qualitatively visible in the 160 K data presented in the configuration snapshot (Fig. 1) and azimuthal distribution (Fig. 7). In the liquid phase we would expect OP_{nem} to vanish, the small finite value in the high temperature phase is an indication of a small residual order likely due to the small system size. Note that contrary to the previous order parameters, OP_{nem} does not vanish due to dynamic fluctuations leading to an overall rotation of the average director over time. We would like to remark that our results for the nematic order parameter (center panel of Fig. 2) differ from those found by Peters and Tildesley (PT)⁸: (a) they find $OP_{nem} \simeq -0.5$ for the HB phase; (b) they find a relatively small $\max[OP_{nem}] \simeq 0.0-0.4$; (c) they find the HB to nematic transition at a higher

temperature (ca. 150 K); and (d) they find a relatively undefined nematic to liquid phase transition at ca. 175 K. The difference in (a) (and to some extent (b)) is due to a factor of 1/2 difference in the definition of ϕ_{dir} in equation (12). The higher “importance” of the nematic mesophase in our work [points (b–d)] we believe is due to the considerably better statistics in our runs (whereas PT used 5×10^4 thermalization and 2×10^5 averaging steps, we typically ran our simulations for $3\text{--}5 \times 10^5$ thermalization and $0.5\text{--}1.0 \times 10^6$ averaging steps).

The tilt order parameter is designed to provide a measure of the out-of-plane orientational order of the system—in particular, the amount of molecular tilting—and is defined as

$$\begin{aligned} OP_{tilt} &\equiv \frac{1}{N_m} \left\langle \sum_{i=1}^{N_m} \langle P_2(\cos \theta_i) \rangle \right\rangle \\ &= \frac{1}{2N_m} \left\langle \sum_{i=1}^{N_m} (3 \cos^2 \theta_i - 1) \right\rangle, \end{aligned} \quad (13)$$

were $P_2(x)$ is the Legendre polynomial and θ_i is the angle that the smallest moment of inertia axis of molecule i makes with the normal to the substrate. Clearly OP_{tilt} is closely associated with the tilt angle distribution $P(\theta)$ (see Fig. 8). When all molecules are parallel to the surface $OP_{tilt} = -0.5$, and $OP_{tilt} = 1$ when all molecules are perpendicular to the surface. The bottom panel of Fig. 2 shows the temperature dependence of OP_{tilt} . At low temperatures the molecules clearly are (as expected) roughly parallel to the graphite substrate to maximize their adsorption energy. At the HB to nematic transition, OP_{tilt} has a significant peak, indicating a tendency of the molecules to librate out of the surface plane, but this tendency is reduced again as the nematic phase is better “established.” For increasing temperatures OP_{tilt} barely increases until the nematic to liquid phase transition, where it starts a significantly faster growth. Tilting of the molecules can obviously be a significant factor in the phase transitions, as the “footprint” of the molecules is reduced. To put things in perspective, however, $OP_{tilt}(200 \text{ K}) \simeq -0.44$ roughly corresponds to an average libration of only 11° out of the plane. Nevertheless, for a full monolayer coverage the resulting “footprint

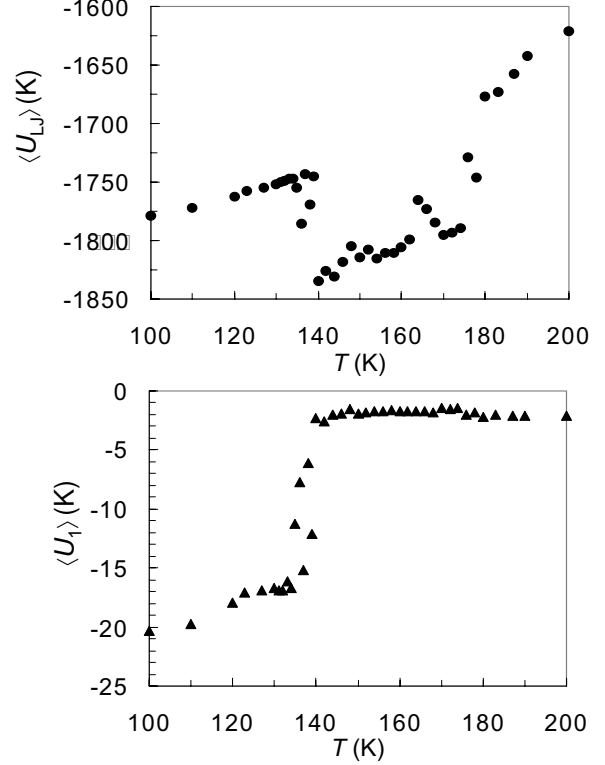


FIG. 3: Thermodynamic information. Ensemble averages per molecule of the Lennard-Jones interaction energy $\langle U_{LJ} \rangle$ and the lateral corrugation in the adsorbate-graphite interaction in Steele’s expansion $\langle U_1 \rangle$. Note the sharp features of $\langle U_{LJ} \rangle$ in both transitions, and the sharp decrease in magnitude of $\langle U_1 \rangle$ at the commensurate-incommensurate/herringbone-nematic transition.

reduction” can be significant. (For more comments on the stiffening of tilting by the substrate potential see Sec. III F.)

B. Energy and Spreading Pressure

In addition to structural indicators shown before (the various order parameters), thermodynamic quantities are helpful in tracking phase transitions. Figure 3 shows the temperature dependence of the average Lennard-Jones interaction energy $\langle U_{LJ} \rangle$ [Eq. (2)] and of the average corrugation potential energy $\langle U_1 \rangle$ [Eqs. (4) and (5)]. The former is useful in delineating the system’s structural behavior irrespective of the substrate’s potential, whereas the latter is a good indicator of atomic order of the substrate and therefore complements the molecular information provided by OP_{comm} (see Sec. III A).

The average interaction energy is very closely related to how close together the hexane molecules are [in fact, $\langle U_{LJ} \rangle \propto \int u_{LJ}(r)g(r)rdr$, where $g(r)$ is the atomic pair correlation function (see Sec. III E)]. The large increase in the magnitude at $T_1 = 138 \pm 2$ K is a clear indication that molecules in the incommensurate nematic phase have managed to become closer to the minimum of the Lennard-Jones interaction. At the melting transition ($T_2 = 176 \pm 3$ K) molecular distances again become less optimal and this average energy rises. Both of these features are evident in the plots of $g_{com}(r)$, see Fig. 11. The average corrugation potential energy $\langle U_1 \rangle$ dramatically decreases in magnitude at T_1 , a clear indication of the lack of registration of the adsorbate film and the substrate.

Other energy ensemble averages have interesting features, but considerably less pronounced than those for $\langle U_{LJ} \rangle$ and $\langle U_1 \rangle$ (typically they show changes in their derivatives with respect to T , but no sudden jumps). One conclusion that can be drawn from the behavior of these energy averages is that the herringbone/commensurate to nematic/incommensurate transition is driven by a competition between the intermolecular forces with the substrate corrugation (see Sec. III F below for more discussion on this).

The specific heat at constant area c_A (not shown) exhibits some scatter, but does present two significant sharp peaks at ca. 138 K and 176 K and there is some indication that there *may* be a latent heat associated with both transitions. However, the energy distributions (not shown) near the transitions do not show any striking bimodality which would seem to suggest that the transition is not first-order. As it is usual with finite-size simulations, the determination of the order of the transitions remains elusive.

Another quantity of interest is the *spreading pressure* (surface “tension”) Φ . The virial expansion²⁰

$$\begin{aligned} \Phi &\equiv \frac{Nk_B T}{A} Z, \\ Z &\equiv 1 + \frac{1}{2Nk_B T} \left\langle \sum_{i \neq j}^N \mathbf{r}_{ij} \cdot \frac{\partial U}{\partial \mathbf{r}_{ij}} \right\rangle \\ &\simeq 1 + \int d^2 r [g_{com}(r) - 1], \end{aligned} \quad (14)$$

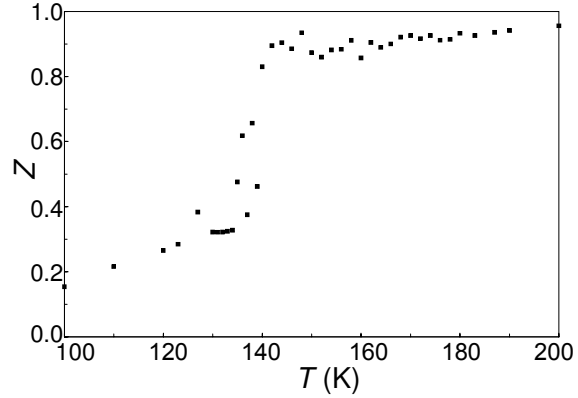


FIG. 4: Relative spreading pressure Z of hexane adsorbed on graphite [see Eq. (14)]. Note that $Z \sim 0$ for $T \lesssim T_1$ as expected for a solid (small spreading pressure), and that Z approaches the ideal gas value ($Z = 1$) for $T \gtrsim T_1$. The value of Z for the intermediate temperature region ($T_1 < T < T_2$) indicates that the nematic is a fluid phase.

relates it to the interactions between molecules or equivalently to the center of mass pair correlation function $g_{com}(r)$ (see Sec. III E). Here N/A is the areal density of the molecules. The “relative spreading pressure” Z is thus a good indicator of how close the equation of state is to that of an ideal gas ($Z \sim 1$) or that of a solid ($Z \sim 0$). Figure 4 shows Z for the hexane system. It is evident from our results that below T_1 the system has a very small spreading pressure as expected for a solid phase, whereas *both* the nematic ($T_1 < T < T_2$) and isotropic phases ($T > T_2$) are very very close to an ideal gas. These results are indicative of the liquid nature of the intermediate nematic phase.

C. Distributions

In conjunction to the order parameters mentioned above, various distributions can also help illustrate the properties of the system, especially near the phase transitions, and in particular regarding the behavior of various molecular degrees of freedom, both positional, orientational and internal. In Figs. 5, 7, 6, and 8 we present the atomic height $P(z)$, azimuthal angle $P(\phi)$, internal roll-angle $P(\psi)$ and tilt angle $P(\theta)$ distributions for various temperatures. For $P(z)$ we considered $0 \leq z \leq 12$ Å sampling every

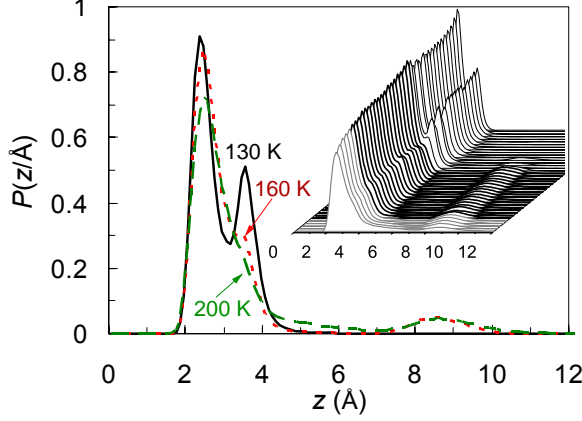


FIG. 5: Atomic height distributions $P(z)$ for the herringbone solid at $T = 130$ K (solid black line); nematic at $T = 160$ K (red dotted line); and liquid at $T = 200$ K (green dashed line). The insert shows all results obtained from $T = 100$ to 200 K back to front respectively. The thin black lines represent the herringbone ($T \lesssim 138$ K), the thick black lines the

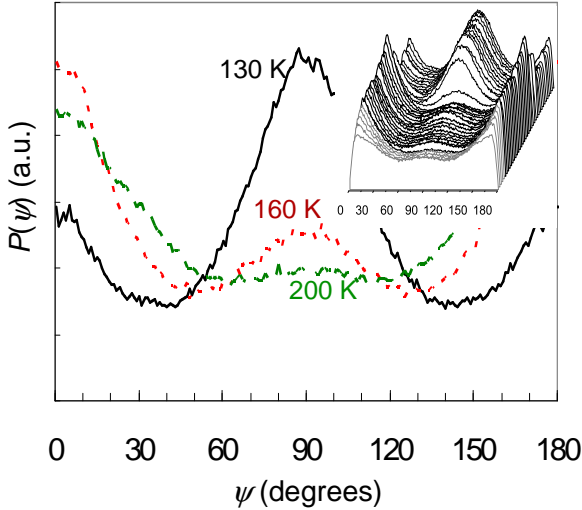


FIG. 6: Molecular roll angle distributions $P(\psi)$. Please refer to Figure 5 for format information. Note how sharp the change in $P(\psi)$ is at the HB to nematic transition.

$\Delta z = 0.0056$ Å. For $P(\phi)$ and $P(\psi)$ and $P(\theta)$ we considered angles the $[0^\circ, 180^\circ]$ domain $\{[0^\circ, 90^\circ]$ for $P(\theta)\}$, sampling every 1° . The azimuthal angle for a molecule, ϕ_i is defined to be the angle formed between the direction of the smallest moment of inertia projected onto the xy -plane and the x axis. The tilt angle θ is defined to be the

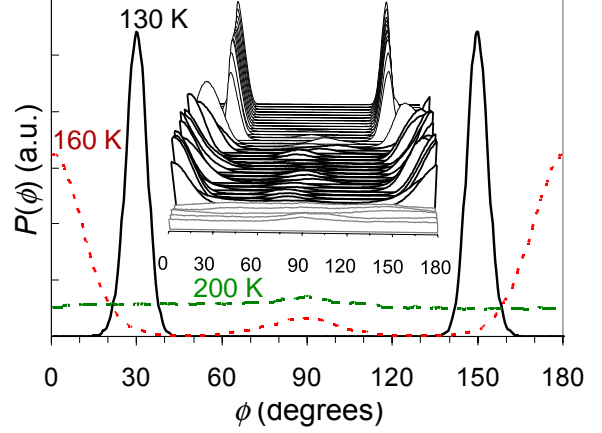


FIG. 7: Molecular azimuthal angle distributions $P(\phi)$. Please refer to Figure 5 for format information. Note how rapidly the position and shape of the peaks change at the HB to nematic transition, and how fast the peaks disappear in the nematic to fluid transition.

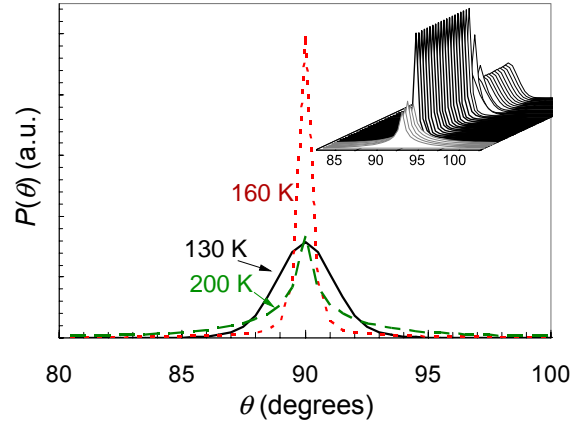


FIG. 8: Molecular tilt angle distributions $P(\theta)$. Please refer to Figure 5 for format information.

angle formed between the direction of the smallest moment of inertia and the z axis ($\theta = 90^\circ$ corresponds to a molecule laying flat on the substrate). The internal roll angle ψ is defined for a particular bond involving any three consecutive atoms as

$$\psi = \cos^{-1} \left\{ \frac{[(\mathbf{r}_{j+1} - \mathbf{r}_j) \times (\mathbf{r}_{j-1} - \mathbf{r}_j)] \cdot \hat{z}}{|(\mathbf{r}_{j+1} - \mathbf{r}_j) \times (\mathbf{r}_{j-1} - \mathbf{r}_j)|} \right\}. \quad (15)$$

The roll-angle has a value of 0 when the plane three consecutive atoms in a molecule is flat (parallel to the graphite basal plane) and it equals 90° when the plane is perpendicular to the graphite²¹.

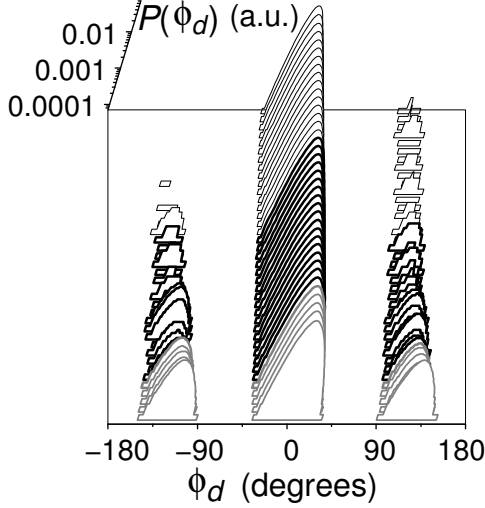


FIG. 9: Dihedral angle distributions $P(\phi_d)$ for $100 \leq T \leq 200$ (back to front). Please refer to Figure 5 for format information.

The atomic height distribution (Fig. 5) shows that essentially no molecules have been promoted to the second layer in the low temperature phase, and only a very small fraction in the nematic or liquid states. The double peak structure at low temperatures can be interpreted easily upon consideration of the molecular roll-angle distributions (Fig. 6): as many molecules are rolled “on their side”, raising some atoms of the hexane chain above the main peak. At higher temperatures molecules are flatter against the surface and the double-peak in $P(z)$ disappears. The azimuthal angle distribution (Fig. 7) shows three distinct temperature regions corresponding to the HB phase for $T \lesssim 138$ K [$P(\phi)$ peaked at 30° and 130°], a nematic for ($138 \text{ K} \lesssim T \lesssim 176 \text{ K}$) [$P(\phi)$ peaked at 0° , but note the presence of a small peak near 90° which corresponds to the formation of domains], and a nearly isotropic fluid for $T \gtrsim 176$ K. A discussion of the tilt angle distribution (Fig. 8) is presented later (Sec. IV D), as it is linked to the mechanisms for the phase transitions. See also the discussion on orientational order parameters in Sec. III A.

D. Internal degrees of freedom

It is important to monitor the degree to which the phase transitions exhibited by the system are

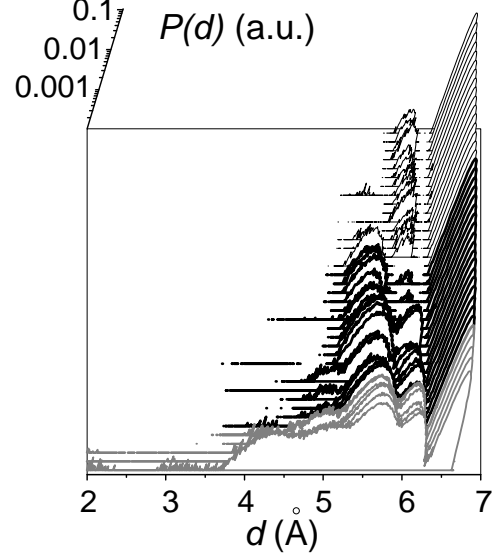


FIG. 10: End-to-end distance distributions $P(d)$ for $100 \leq T \leq 200$ (back to front). Please refer to Figure 5 for format information.

correlated to internal degrees of molecular freedom. The bond-angle distribution (not shown) is a simple gaussian corresponding exactly to the Maxwell-Boltzmann distribution for the potential u_{bend} [Eq. (6)]. This is, in fact, indicative that the bond angles are unaffected by interactions with other molecules or substrate and irrelevant to the properties of the phases and phase transitions studied. Figures 9 and 10 show the distributions of the dihedral angles, $P(\phi_d)$, as well as end-to end distances (CH₃-CH₃ separations in the same molecule), $P(d)$, respectively.

The information on both figures is significantly correlated, as the lower-length molecules correspond to the presence of one or more gauche defects [the width of the main lobe in $P(d)$ corresponds to the width of the bond-angle distribution]. We find that the number of gauche defects is significantly smaller than for hexane molecules *in vacuo* [equipartition based on u_{tors} , Eq. (7)], mostly due to the “flattening effect” of the substrate potential, but also due to the interactions with the neighbors to a lesser degree. The number of gauche defects is small until close to T_2 and does not present a very significant temperature dependence. The end-to-end probability distribution shows a slightly more pronounced change at T_1 . Given that the fraction

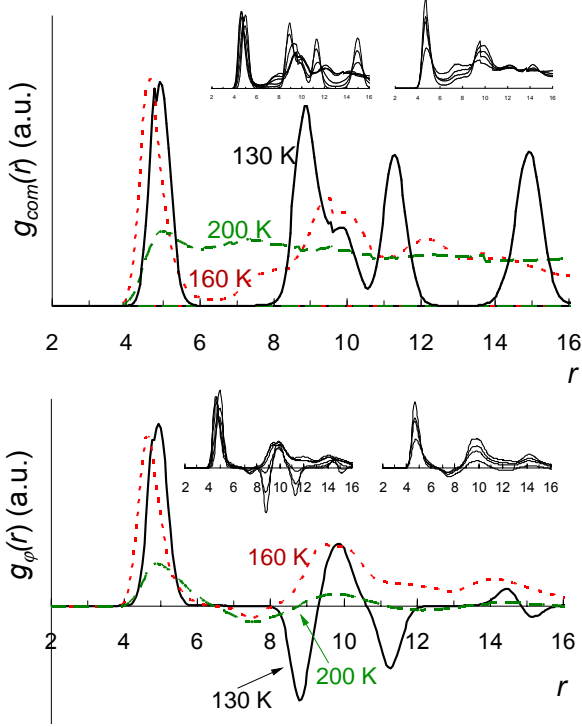


FIG. 11: Center of mass molecular pair correlation function $g_{com}(r)$ (top panel) and molecular orientational pair correlation function $g_{\phi}(r)$ for the herringbone solid at $T = 130$ K (solid black line); nematic at $T = 160$ K (red dotted line); and liquid at $T = 200$ K (green dashed line). The left inserts show the transitional region between herringbone and nematic ($130 \text{ K} < T < 150 \text{ K}$), the right inserts show the transitional region between nematic and liquid ($170 \text{ K} < T < 180 \text{ K}$).

of molecules involved (those with gauche defects) is so small, we find it unlikely that these internal degrees of freedom affect significantly the phase transition at T_1 . For the phase transition at T_2 we find that gauche defects do contribute to the footprint reduction as first suggested by Hansen *et al.*^{4,5}, however that contribution does not appear to be as important as that from tilting (see Sec. IIIF).

E. Correlations

We have also obtained various correlation functions that permit a more complete elucidation of the characteristics of the three phases observed for hexane on graphite and to calculate properties that can be directly probed experimentally [i.e. the static structure factor $S(q)$, see

below].

We start by defining the center of mass molecular pair correlation function $g_{com}(r)$, which corresponds to the joint probability of finding a molecule with center of mass a distance r away from another. We also define the *orientational* pair correlation function $g_{\phi}(r)$, which is calculated by averaging $\cos 2(\phi_j - \phi_i)$ (ϕ_i is the azimuthal angle of the i -th molecule) calculated over all molecule pairs (i, j) whose centers of mass have a separation r . (In practice correlation functions are calculated on a discrete sampling of the distance between the centers of mass, in our case we used $\Delta r = 0.083 \text{ \AA}$, also note that we use two-dimensional normalization.)

Figure 11 presents $g_{com}(r)$ and $g_{\phi}(r)$ for various relevant temperatures. For 130 K, both curves confirm that the HB phase is solid [$g_{com}(r)$ has a sharp peak structure and vanishes between peaks], and the sharp alternating signs of $g_{\phi}(r)$ is indicative of the HB phase too. At 160 K, however, the correlation functions reveal that the mesophase is, indeed, liquid, but with a very strong *orientational order* corresponding to a nematic phase. The evidence is quite strong towards labeling the mesophase as a *nematic liquid crystal*. At 200 K, $g_{com}(r)$ is rather smooth and $g_{\phi}(r)$ rapidly decays to 0, a clear indication of a regular liquid behavior. This behavior is consistent with the conclusions obtained from the analysis of the spreading pressure in Sec. IIIB (see Fig. 4).

A second important correlation function corresponds to the *atom-atom* pair correlation function $g(r)$ which is defined as the joint probability of finding one *atom* at a distance r from another (again, distances were discretized with $\Delta r = 0.083 \text{ \AA}$, and we used two-dimensional normalization). Figure 12 shows the atomic pair correlation function for three characteristic temperatures corresponding to a HB (130 K), a nematic (160 K) and a liquid (200 K). In all cases, we observe very sharp peaks corresponding to intramolecular pairs: $r = 1.54, 2.58, 3.96, 5.16$ and 6.50 \AA which correspond exactly to the atomic distances in a hexane molecule in its lowest configurational state. Broader (and weaker) peaks (visible only in the lower panel) at small distances correspond to intramolecular pairs af-

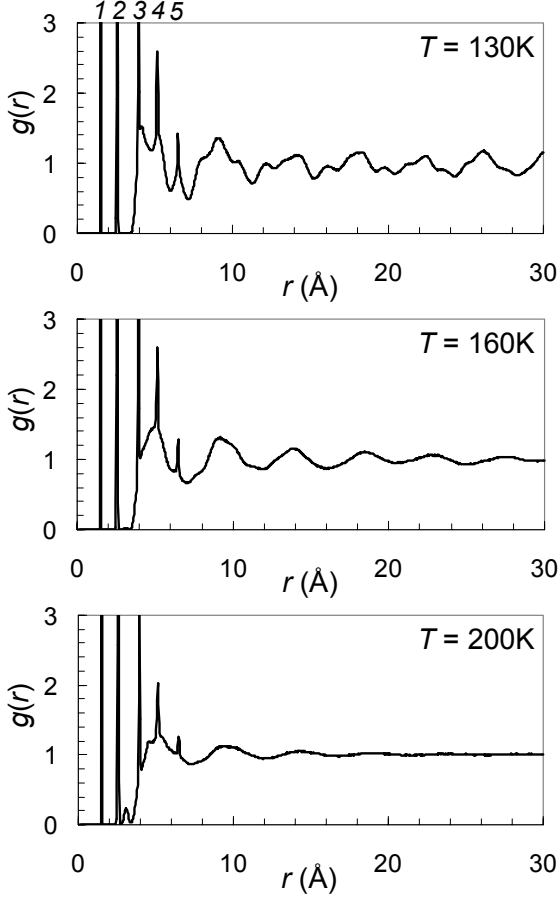


FIG. 12: Atomic pair correlation function $g(r)$ for the Herringbone solid (top panel, $T = 130\text{ K}$), nematic (middle panel, $T = 160\text{ K}$), and liquid (bottom panel, $T = 200\text{ K}$). The sharp peaks numbered 1–5 correspond to intramolecular pairs at distances corresponding to a hexane molecule in its lowest configurational state: $r = 1.54, 2.58, 3.96, 5.16$ and 6.50 Å. Broader (and weaker) peaks (visible only in the lower panel) at small distances correspond to intramolecular pairs affected by a gauche defect: $r = 3.11, 4.55$ and 6.05 Å. The broad and relatively smooth behavior at larger distances corresponds to pairs belonging to different molecules.

affected by a gauche defect: $r = 3.11, 4.55$ and 6.05 Å. The broad and relatively smooth behavior at larger distances corresponds to pairs belonging to different molecules.

From the atomic pair correlation function, one can readily obtain the static structure factor $S(q)$ which is very important because it contains spectral weight information in reciprocal space, and is therefore directly connected to experimental diffraction data^{2–6}. Since most experiments

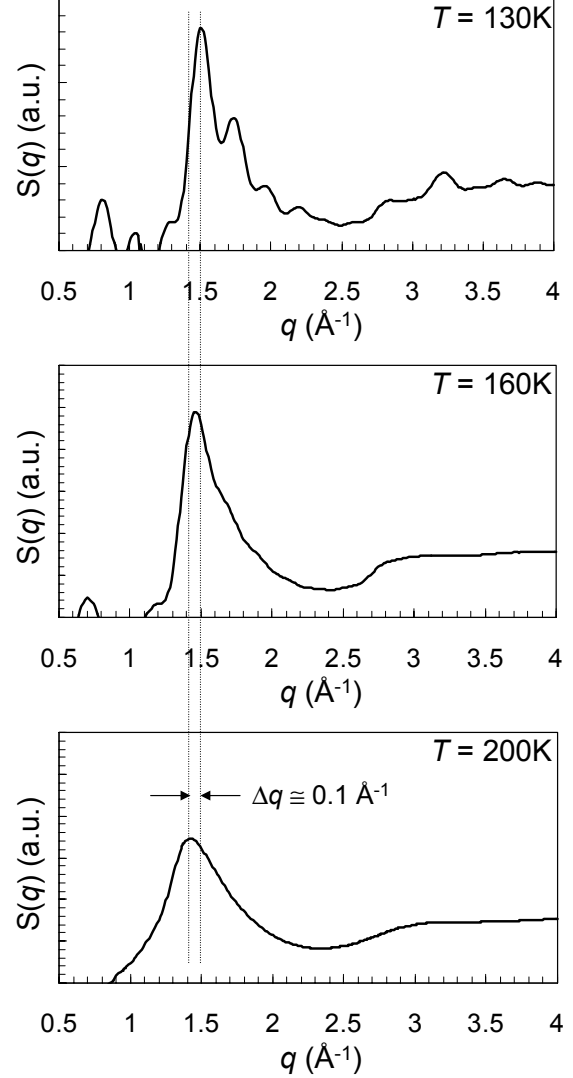


FIG. 13: Static structure factor $S(q)$ for the Herringbone solid (top panel, $T = 130\text{ K}$), nematic (middle panel, $T = 160\text{ K}$), and liquid (bottom panel, $T = 200\text{ K}$).

are performed with powder samples, we chose to calculate a three-dimensionally averaged static structure factor:

$$S(q) = 1 + \int_0^\infty \frac{\sin qr}{qr} [g(r) - 1] r dr. \quad (16)$$

Figure 13 presents the static structure factor calculated from the atomic pair correlation functions in Fig. 12. We note a general broadening of $S(q)$ with increased temperature and only a rather minor shift towards smaller momenta of the main peak. The results are in qualitative agreement with experimental evidence^{2–6}.

F. Variations

In order to better understand the nature of the phase transitions (in particular the less well known HB to nematic) we ran MD simulations where some of the interaction potentials were varied. We considered three interesting possibilities: (a) variations of the Lennard-Jones interaction parameter ϵ_{CH_2} and ϵ_{CH_3} corresponding to the pseudo atoms of the hexane molecules [Eq. (2)], from 25% to 200% of its “standard” value; (b) variations of the corrugation potential strength in Steele’s expansion [Eqs. (4) and (5)], from 25% to 1,000% of the commonly accepted strength. ; and (c) variations of the dihedral potential strength $u_{\text{tors}}(\phi_d)$ [Eq. (7)] from its usual strength (Table II) to ten times higher thus effectively eliminating gauche defects.

We find that for the first type of variations [item (a) above], both T_1 (the HB to nematic transition) and T_2 (the nematic to isotropic liquid transition) scale roughly like $\epsilon_{\text{CH}_n}^{1/2}$ with a correlation $R^2 \simeq 0.999$. As $T_2 - T_1$ increases for larger ϵ_{CH_n} the nematic has a better chance of “expressing itself” and the maximum value of OP_{nem} increases too. This simple scaling indicates that the substrate-atom interaction [mostly through the $E_{0i}(z_i)$ term—see Eq. (4), which holds the molecules stronger to the surface stifling tilting] is dominant in setting the temperature scales [since Lorentz-Bertholt rules, Eq. (3), makes this interaction scale like $\epsilon_{\text{CH}_n}^{1/2}$]. The reason the holding potential influences the phase transitions directly can be attributed to its stifling effect on tilting and the formation of gauche defects.

In the second type of variations [item (b) above], we find that T_1 increases with the corrugation energy, whereas T_2 is almost insensitive to it. As T_1 increases, the nematic phase becomes “weaker”, eventually disappearing for a corrugation ca. 5 times the standard value, and we see a direct transition between the HB and the isotropic fluid. These observations demonstrate that the corrugation is irrelevant for the nematic to isotropic melting (as expected, since this transition occurs between two incommensurate phases). Furthermore, the increase of T_1 is an indication that, in addition to the effect of

holding potential described above, a competition between the corrugation potential (which favors a commensurate phase) and the interactions between molecules (which favors some *other* characteristic intermolecular spacing) is important.

The third type of variation [item (c) above] is useful to characterize which degrees of freedom contribute to the footprint reduction mechanism that creates in-plane space that facilitates the phase transitions. Since the transition at T_1 happens when the number of gauche defects is minuscule, it is evident that they are not important there. For the phase transition at T_2 we found (Sec. III) a significant increase in tilting *and* gauche defects as the system achieves its high temperature phase. Our variation of $u_{\text{tors}}(\phi_d)$, which essentially eliminates gauche defects, resulted in an increase of T_2 by ca. 20 K. This clearly indicates that gauche defects are important for the footprint reduction as first suggested by *et al.*^{4,5}, however tilting appears to be more important.

IV. DISCUSSION

A. Herringbone commensurate solid to nematic liquid crystal transition at $T_1 = 138 \pm 2$ K

The low temperature ($T \lesssim 138$ K) phase of the hexane on graphite system is a commensurate herringbone solid, as evidenced by the structure shown in Fig. 1, the values of OP_{herr} , OP_{comm} and OP_{nem} in Figure 2, and the two distinct peaks in the azimuthal angle distribution $P(\phi)$ at 30° and 150° in Fig. 7. The spreading pressure of this solid system is very small (low temperature region of Fig. 4). Since the monolayer is complete the system creates in-plane room by the molecules spending a significant amount of their time rolled on their side, as seen in the large peak in the roll angle distributions $P(\psi)$ in Fig. 6 as well as the double-peaked atomic height distribution $P(z)$, see Fig. 5.

As the temperature of the system is increased, the usual signatures of increasing thermal fluctuations appear, up until $T_1 = 138 \pm 2$ K, where the system undergoes a phase change. Together, the structural order parameters in Fig-

ure 2 indicate that the system becomes incommensurate at the same time it loses its herringbone orientational ordering. In fact, this is also confirmed by the sharp decrease in magnitude in the average Steele corrugation energy $\langle U_1 \rangle$ (Fig. 3, bottom panel) indicates that, even for atomic degrees of freedom the system is incommensurate. The center of mass pair correlation function $g_{com}(r)$ (Fig. 11, top panel) indicates that the new phase is fluid, as evidenced by the fact that $g_{com}(r)$ has relatively smooth features, and that the molecules are slightly closer to one another, which also leads to an increase in the magnitude of the interaction energy $\langle U_{LJ} \rangle$ (Fig. 3, top panel). The liquid nature of this phase is also evidenced by the relatively large spreading pressure (Fig. 4). As the solid-nematic transition proceeds, the tilt angles of the molecules fluctuate creating a footprint reduction that facilitates the phase transition (yet tilting is once again reduced when the new phase is reached), as seen by the sharp peak in OP_{tilt} at ca. 138 K (Fig. 2, bottom panel).

Inspection of the snapshots in Fig. 1, plus more quantitative considerations based on OP_{nem} and $P(\phi)$ further indicates that the positional order lost in this phase transition occurs simultaneously with a new orientational order where all molecules have a common director. The molecules experience, in fact, a relatively long range orientational order (see 160 K curve, Fig. 11, bottom panel). We believe that this phase has all the characteristics of a two dimensional *nematic liquid crystal*. Analysis of the probability distributions for the bond and dihedral angles, and for the molecular end-to-end distance indicate that the internal degrees of freedom do not cooperate significantly with the HB to nematic phase transition. In fact, it seems that they hardly participate at all in the relevant processes in the temperature range studied for a monolayer of hexane adsorbed on graphite. It should be noted that number of gauche defects is significantly smaller than what would be predicted *in vacuo*, which is due to a large degree to the substrate interaction, and to a lesser degree to the interaction between molecules which has an aligning effect.

B. Nematic to isotropic liquid phase transition at $T_2 = 176 \pm 3$ K

As the temperature is raised, the nematic persists up until $T_2 = 176 \pm 3$ K where another orientational phase transition occurs, this time to an isotropic fluid. The phase transition is characterized by a sudden drop in the nematic order parameter OP_{nem} (Fig. 2, center panel) and the disappearance of any directional preference in the azimuthal angle distribution $P(\phi)$ (Fig. 7, see also the random orientation in the 200 K snapshot in Fig. 1). In addition, the orientational pair correlation function $g_\phi(r)$ shows that angular correlations between molecules decay extremely rapidly with distance in the high temperature phase (see 200 K curve, Fig. 11, bottom panel). The Lennard-Jones interaction increases sharply (which is related to the increase in the typical intermolecular distances), and there is a strong peak at T_2 in the specific heat c_A .

In the liquid, the tilt angle behavior shown in the bottom panel of Fig. 2 reveals that the molecular axes are much freer to fluctuate than in the nematic and this may cause a significant reduction in the molecular footprint (as discussed in Sec. III F, gauche defects also contribute to this footprint reduction, though tilting appears to be more important). The dihedral angle and end-to-end distance distributions in Figs. 9 and 10 show that, in the liquid, gauche and other dihedral defects are promoted more readily with increasing temperature, but, as with the solid-to-nematic phase transition, no new or abrupt changes in the internal degrees of molecular freedom accompany melting.

C. Information related to scattering

The atomic pair correlation functions in Fig. 12 are a combination of intra- and intermolecular pair terms and hence are rich in information about how the internal degrees of freedom behave as well as the bulk structure of the system's phase. The five extremely sharp peaks correspond to atom-atom distances within the molecules, and correspond precisely to the intramolecular atomic distances in the ground state of hexane. Careful inspection of the

$g(r)$ curves at high temperatures reveals the emergence of smaller more diffuse peaks, which again precisely correspond to the intramolecular atomic distances, this time in presence of one gauche defect. When the curve $g(r)$ starts to elevate off the horizontal axis, the contribution from atom pairs between different molecules begins and the decreasing structural order with increasing temperature is evident. The static structure factor $S(q)$ shown in Fig. 13 helps further understand the behavior of $g(r)$. We note a general broadening of $S(q)$ with increased temperature and only a rather minor shift towards smaller momenta of the main peak. The results are in qualitative agreement with experimental evidence²⁻⁶.

D. Mechanisms

As in previous computer simulations⁷⁻⁹, our work reproduces general features of the real system as explored by experiment, and quite accurately determines the melting temperature T_2 ¹⁻⁶. Our findings of an intermediate *nematic* liquid crystalline phase between T_1 and T_2 are roughly in agreement with previous simulations by Peters and Tildesley⁸. However, the existence of this intermediate phase has not been confirmed experimentally, which suggests that larger computer simulations would be of interest in determining the presence of highly complicated domain behavior, or even dynamic domains that smaller simulations simply cannot capture.

A unique benefit of computer simulations is that they allow careful inspection of the mechanism for various phase transitions when enough data is present. In the work presented here, we see that in the solid herringbone phase the molecules spend much time rolled so that their backbones are ziz-zagged, or rough relative to the graphite substrate (see Fig. 6). The solid to nematic transition involves negligible amount of gauche defects (Fig. 9), instead showing pronounced molecular tilt fluctuations (Fig. 2, bottom panel) in concert with the molecules' rolling on their sides. The resulting nematic phase still has an average density of unity but the molecules are closer to each other (in the direction perpendicular to the molecules), as evidenced by the shift in the first peak of the cen-

ter of mass pair distribution function $g_{com}(r)$ (Fig. 11) and the sudden increase in magnitude of the Lennard-Jones interaction $\langle U_{LJ} \rangle$ (Fig. 3, top panel). As a result, the tilt-angle distribution (Fig. 8) takes on a fundamentally different shape somewhat more sharply peaked than the gaussian-like distributions seen in the solid. The importance of the molecule-molecule interaction in the mesophase is underscored by the fact that the tilt angle distributions do not considerably broaden in the nematic.

At a higher temperature the system melts onto an isotropic phase. Although no sudden increase in tilt fluctuation accompanies melting, the tilt angle distributions begin to show thermal broadening, accounting for the increased slope of OP_{tilt} in the liquid (Fig. 2, bottom panel). A possible "signature" of the nematic is that the tilt angles are locked and that it is a "tilt-locking" mechanism that precedes the mesophase. The first simulations completed on the system^{4,5} concluded that, at melting, proliferation of dihedral (gauche) defects in the adsorbate cause the projected presence of the molecules (their footprint) to decrease, thus creating more in-plane room for center-of-mass molecular fluctuations and thus allowing melting to ensue. In fact, freezing of the dihedral degrees of freedom resulted in a considerable increase in the system's melting temperature. Later work by the same authors⁶ and others⁷⁻⁹ suggests that, when the molecule-substrate interaction strength is decreased to more realistic values, gauche defects become unimportant for melting. Our work suggests that the creation of in-plane free space is indeed important for all phase transitions in the system, but that the "footprint reduction" happens exclusively through tilting (and moderate stacking) at the solid-nematic transition, where the internal molecular degrees of freedom are unimportant. The "footprint reduction" for the nematic-isotropic transition is, indeed, caused by both gauche defects and tilting, as both the probability of finding significant dihedral angles *and* tilting start rising significantly near T_2 (see bottom panel of Fig. 2 and Fig. 9).

The simulations conducted on the variation of various Lennard-Jones interaction parameters

agree with the above assessments because when only the lateral graphite corrugation well depth is varied [type (b) as defined in Sec. IIIF], T_1 increases slightly and T_2 remains unchanged. However when the potential parameters for the pseudoatoms themselves are varied [type (a)], the interaction of the adatoms with the substrate also increases, including a stronger vertical force component. Thus, tilting is stifled and T_1 and T_2 are significantly affected. Since we already know that an increase in lateral forces alone cause relatively small changes in T_1 , such results underscore the importance of tilting prior to the nematic. Our elimination of gauche defects by varying the torsional potential [variation type (c)] resulted in a moderate increase of the transition temperature T_2 , from which we conclude that both tilting and gauche defects are significant, albeit it seems that the former are more important. In essence, we agree qualitatively with earlier work's findings that "footprint reduction" is important in this system, only in our work the prevalent mechanism is tilting.

E. Final Remarks

Our simulations indicate that the HB to nematic transition is due to a competition between the pro-commensurate interaction between adsorbate molecules and the corrugation substrate potential and the intermolecular interactions which favors intermolecular distances different from the required by the substrate. The latter prevail at ca. 138 K, leading to a nematic liquid crystalline state. If a stronger attraction to the substrate is used in our simulations (Sec. IIIF) the stifling of mechanisms that reduce the molecular footprint makes the phase transition occur at a higher temperature. An increase in the corrugation potential has a similar effect. The

nematic to isotropic transition is, as expected, rather insensitive to the corrugation potential, but remains very sensitive to the main part of the substrate-adatom potential.

We have observed somewhat contradictory evidence in terms of trying to identify the order of the phase transitions. Whereas the specific heat curves seem to indicate that there may be a latent heat in both cases, the lack of bimodality in the energy distributions would indicate otherwise. The inconclusiveness is not, however, surprising given the finite size of the system simulated.

We have also performed MD simulations with ca. $2\times$ and $4\times$ the number of molecules discussed throughout this paper. We find that the HB to nematic phase transition temperature T_1 is only weakly dependent on system size (but the relatively poor statistics possible with the larger sizes make it difficult to extrapolate to the thermodynamic limit). The nematic to isotropic phase transition temperature T_2 is insensitive to system size for the sizes considered.

Acknowledgments

The authors are indebted to Haskell Taub, Flemming Hansen, Günter Peters, Peter Pfeifer, Cintia Lapilli and James MacCollough for enriching discussions. Acknowledgement is made to the Donors of the Petroleum Research Fund, administered by the American Chemical Society, for support of this research. CW acknowledges support from the University of Missouri Research Board and the University of Missouri Research Council. MR and CP acknowledge support by the University of Northern Iowa Faculty Summer Research Fellowship and University of Northern Iowa Summer Undergraduate Research Fellowship respectively.

-
- ¹ J. Krim, J. Suzanne, H. Shechter, R. Wang and H. Taub, *Surf. Sci.* **162**, 446 (1985).
 - ² J.C. Newton, P.D. dissertation, University of Missouri-Columbia (1989), unpublished.
 - ³ H. Taub, *NATO Advanced Study Institutes, Series C: Mathematical and Physical Sciences*, vol. 228,

edited by G. J. Long and F. Grandjean (Kluwer, Dordrecht, 1988), pp. 467-497.

- ⁴ F.Y. Hansen and H. Taub, *Phys. Rev. Lett.* **69**, 652 (1992).
- ⁵ F.Y. Hansen, J.C. Newton and H. Taub, *J. Chem. Phys.* **98**, 4128 (1993).

- ⁶ K.W. Herwig, Z. Wu, P. Dai, H. Taub, and F.Y. Hansen, J. Chem. Phys. **107**, 5186 (1997).
- ⁷ E. Velasco and G.H. Peters, J. Chem. Phys. **102**, 1098 (1995).
- ⁸ G.H. Peters and D.J. Tildesley, Langmuir **12**, 1557 (1996).
- ⁹ G.H. Peters, Surf. Sci. **347**, 169 (1996).
- ¹⁰ J.M. Kosterlitz and D.J. Thouless, J. Phys. C. **6**, 1181 (1973).
- ¹¹ J.M. Kosterlitz, J. Phys. C. **7**, 1096 (1974).
- ¹² B.I. Halperin and D.R. Nelson, Phys. Rev. Lett. **41**, 121 (1978).
- ¹³ D.R. Nelson and B.I. Halperin, Phys. Rev. B **19**, 2457 (1979).
- ¹⁴ K.J. Strandburg, Rev. Mod. Phys. **60**, 161 (1988).
- ¹⁵ M.P. Allen, D.J. Tildesley, *Computer simulation of liquids*, Clarendon Press (New York, 1988).
- ¹⁶ M.G. Martin, and J.I. Siepmann, J. Phys. Chem. **102**, 2569 (1998).
- ¹⁷ W.A. Steele, Surf. Sci. **36**, 317 (1973).
- ¹⁸ P. Padilla and S. Toxværd, J. Chem. Phys. **94**, 5650 (1991).
- ¹⁹ Note that since hexane is not polar, we are dealing with *directors* rather than vectors, hence the $[0, \pi]$ range for ϕ_i , similar arguments also apply to other molecular directions ($\theta_i \in [0, \pi/2]$, $\psi \in [0, \pi]$).
- ²⁰ See e.g. M. Plischke and B. Bergersen, *Equilibrium Statistical Physics* 2nd. Ed. (World Scientific, Singapore, 1994), Chapters 4 and 7.
- ²¹ The internal roll angle is related to the rolling angle in previous work^{8,9}, with the exception that it gives information about the rotation of the planes that each bond angle lies in as opposed to overall molecular orientation.